Seventh Symposium on Salt, Vol. I 105–115 (1993)
Elsevier Science Publishers B.V., Amsterdam

Constitutive Equation for Rock Salt and Mining Applications

N. Cristescu*

Department of Mechanics, Bucharest University, Romania

ABSTRACT

This paper presents a non-associated elastic/viscoplastic constitutive equation for rock salt formulated for general triaxial stress states. This constitutive equation can describe creep, dilatancy and/or compressibility, work-hardening, progressive damage, creep failure and sudden failure, all being incorporated in the constitutive equation. This equation is then used to predict where, around a horizontal tunnel, the rock will become either dilatant, compressible, or maybe elastic, or where a failure will occur. Depths in the range 1–1.5 km were considered with two possible pressures exerted on the wall, namely an empty tunnel (no internal pressure) and pressure due to a filling with brine.

Creep around vertical shafts or caverns is another problem considered. It is shown how the dilatancy domain enlarges with depth, where failure is possible, and how radial convergence varies with depth. Complete closure is possible at the greater depths. The influence of the pressure exerted by a brine column is also considered.

INTRODUCTION

The determination of general and accurate constitutive equations for rock salt is a subject of much concern and for obvious reasons, namely improvement of mining procedures and design of large underground cavities for storage of hydrocarbons or for radioactive wastes or hazardous chemical wastes. For various types of constitutive equations the reader is referred to those formulated by Serata et al. (1972), Albrecht and Langer (1974), Albrecht and Hunsche (1980), Wawersik et al. (1982), Horseman and Passaris (1984), the BGR model presented by Langer (1984), Munson and Dawson (1984), Wawersik and Zeuch (1986), Desai and Varadarajan (1987), Aubertin et al.(1989, 1991), Blum et al. (1989), Hunsche (1990a,b), Spiers and Schutjens (1990) and Vogler and Blum (1990). The book by Dreyer (1973) is also to be mentioned.

Generally, in most existing approaches, a uniaxial constitutive equation is first established which is then generalized for triaxial stress states. A different approach is used by the present author (Cristescu 1987, 1989, 1991, 1992). The general triaxial constitutive equation is established directly for triaxial stress states starting from a complete set of triaxial experimental data. The procedure allows for the determination of a non-associated elastic/viscoplastic constitutive equation able to describe creep, dilatancy and/or volume compressibility during creep, work-hardening, evolutive damage, creep failure and ultimate failure. All these properties can be incorporated in the constitutive equation. Thus one can very easily use this constitutive equation for the design of underground structures.

Starting from a very accurate and complete set of data obtained in 'true' triaxial tests by Hunsche (1988, personal communication: 1991), two variants of such constitutive equations have already been formulated by Cristescu and Hunsche (1991, 1992) and Cristescu (1993). In the this paper another variant obtained with a greater quantity of experimental data, which were corrected for experimental errors, will be used. This variant of the constitutive equation will be presented in detail in a forthcoming paper by the same two authors.

THE CONSTITUTIVE EQUATION

General aspects

The constitutive equation is of a phenomenological elastic/viscoplastic type and is of the form used already for several other rocks (Cristescu 1987, 1989). The reference configuration, with respect to which the strains produced by an excavation are to be evaluated, is the state *in situ* before excavation at

* Present address: Department of Engineering Sciences, University of Florida, Gainesville, FL, USA.

the future location. Using conventional notation for the strain rate and Cauchy stress tensors, this constitutive equation reads

$$\dot{\varepsilon} = \frac{\dot{\sigma}}{2G} + \left(\frac{1}{3K} - \frac{1}{2G}\right)\dot{\sigma}\,\mathbf{1} + k\left\langle 1 - \frac{W^I(t)}{H(\sigma)}\right\rangle \frac{\partial F}{\partial \sigma} \qquad (1)$$

Here G and K are the elastic parameters (shear and bulk moduli) which may depend on stress, strain and possibly on a damage parameter, the relation

$$H(\boldsymbol{\sigma}) = W^I(t) \qquad (2)$$

is the equation of the stabilization boundary (where $\dot{\varepsilon} = 0$ and $\dot{\boldsymbol{\sigma}} = 0$) for the transient creep with $W^I(t)$ a work-hardening parameter defined below, $F(\boldsymbol{\sigma})$ is a viscoplastic potential generally distinct from the yield function $H(\boldsymbol{\sigma})$ (see Cristescu, 1991), and k is a coefficient so that $k(\partial F/\partial \boldsymbol{\sigma})$ can be considered a 'variable viscosity coefficient', with k playing the role of the magnitude of this viscosity coefficient. Further, 1 is the Kronecker unit tensor, the term

$$\sigma = \frac{1}{3}(\sigma_1 + \sigma_2 + \sigma_3) \qquad (3)$$

is the mean stress and

$$\tau = \frac{1}{3}\left[(\sigma_1 - \sigma_2)^2 + (\sigma_2 - \sigma_3)^2 + (\sigma_3 - \sigma_1)^2\right]^{1/2} \qquad (4)$$

is the octahedral shear stress related via $\tau = [2/3\ II_{\sigma}]^{1/2}$ to the second invariant ($II_{\sigma'}$) of the stress deviator; we have also $\bar{\sigma}^2 = 3\ II_{\sigma'}$ with $\bar{\sigma}$ the equivalent stress. In addition, the above-mentioned work-hardening parameter or internal state variable $W^I(t)$ is the stress power defined as

$$W^I(T) = W^{IP} + \int_0^T \sigma(t)\dot{\varepsilon}_v^I(t)\ dt + \int_0^T \boldsymbol{\sigma}'(t)\cdot\dot{\boldsymbol{\varepsilon}}^{I'}(t)\ dt \qquad (5)$$

where $T = 0$ is the moment of the beginning of excavation, W^{IP} is the initial (primarily existing) stress power, $\dot{\varepsilon}_v^I$ is the irreversible volumetric rate of deformation, and prime stands for 'deviator'. Finally, the notation

$$\langle A\rangle = A^+ = \frac{1}{2}(A + |A|)$$

is the positive part of A.

All the constitutive parameters and functions involved in (1) are determined from the data obtained in true triaxial tests. At this stage of development of the model we assume that both constitutive functions H and F depend on the two stress invariants σ and τ, only.

In order to understand well how the above model can describe dilatancy or compressibility during creep, we write the volumetric rate of deformation as

$$\dot{\varepsilon}_v^I = k\left\langle 1 - \frac{W^I(t)}{H(\sigma,\tau)}\right\rangle \frac{\partial F(\sigma,\tau)}{\partial \sigma} \qquad (6)$$

Figure 1 shows typical surfaces corresponding to H = constant and F = constant, together with the compressibility ($\partial F/\partial\sigma > 0$) and dilatancy ($\partial F/\partial\sigma < 0$) domains. Generally, for most rocks, ultimate failure is loading rate dependent: high loading rates produce failure at higher values of τ and smaller strains at failure, and vice versa. What the influence would be of the loading rate on failure is not yet well established for rock salt

Let us assume that the primary stress state (the stress existing *in situ* before excavation) is represented by the point P in Fig. 1. We assume that this stress state is an equilibrium state, i.e. $H(\boldsymbol{\sigma}^P) = W^{IP}$. Due to the excavation, the stress changes from $\boldsymbol{\sigma}^P(t_0)$ to $\boldsymbol{\sigma}(t)$. The new stress state is represented by a point which may belong to any region shown in Fig. 1.

We can now distinguish the following cases. If

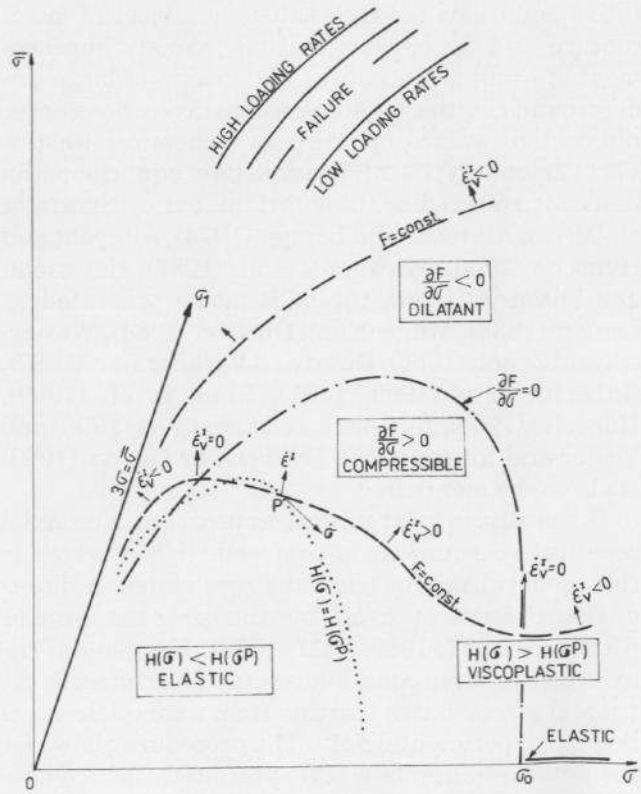

Fig. 1. Various domains in stress space of dilatancy, compressibility, elasticity and failure.

$$H(\boldsymbol{\sigma}(t)) < H(\boldsymbol{\sigma}^P) \tag{7}$$

the response of the rock is *elastic*. If however

$$H(\boldsymbol{\sigma}(t)) > H(\boldsymbol{\sigma}^P) \tag{8}$$

the new stress state is in the *viscoplastic* region, with various possible cases:

$$\frac{\partial F}{\partial \sigma} > 0 \quad \text{compressibility} \tag{9}$$

$$\frac{\partial F}{\partial \sigma} = 0 \quad \text{compressibility/dilatancy boundary} \tag{10}$$

$$\frac{\partial F}{\partial \sigma} < 0 \quad \text{dilatancy} \tag{11}$$

all depending on the orientation of the normal to the surface F = constant, passing through the point representing the actual stress state, as shown in Fig. 1. Thus, once the constitutive function is determined, all these possible cases are well determined, as will be shown in the examples given below.

Constitutive parameters and functions for rock salt

For rock salt the constitutive parameters and functions involved in (1) have been determined experimentally (Hunsche, 1991, personal communication) and will be discussed in detail in a paper by Hunsche and Cristescu (1993). They are summarized here as follows:

(A) the elastic parameters in unloading tests are E = 30 GPa, K = 21.7 GPa, G = 11.8 GPa and $\nu = 0.27$;

(B) the yield function

$$H(\sigma,\tau) := \sigma_* \left\{ \exp\left[a_1\left(\frac{\sigma}{\sigma_*}\right)^2 + a_2\frac{\sigma}{\sigma_*} + a_3\right]\right\}\left(\frac{\tau}{\sigma_*}\right)^9 + \left\{b_1\left(\frac{\sigma}{\sigma_*}\right)^2 + b_2\frac{\sigma}{\sigma_*} + b_3\right\}\left(\frac{\tau}{\sigma_*}\right) + \left\{c_1\left(\frac{\sigma}{\sigma_*}\right)^2 + c_2\frac{\sigma}{\sigma_*} + c_3\right\}\frac{\tau}{\sigma_*} + \begin{cases} h_1\sigma^2 & \text{if } \sigma \le \sigma_A \\ h_2\sigma + h_3 & \text{if } \sigma \ge \sigma_A \end{cases} \tag{12}$$

with
$a_1 = 4.5\cdot10^{-3}$, $b_1 = -4.7\cdot10^{-6}$ MPa, $c_1 = 4.46\cdot10^{-5}$ MPa, $a_2 = -0.35$, $b_2 = 3.13\cdot10^{-4}$ MPa, $c_2 = 2.65\cdot10^{-3}$ MPa, $a_3 = -21.9$, $b_3 = -2.65\cdot10^{-3}$ MPa, $c_2 = 4.78\cdot10^{-2}$ MPa, $h_1 = 4.6\cdot10^{-4}$ (MPa)$^{-1}$, $\sigma_* = 1$ MPa, $h_2 = 5.56\cdot10^{-3}$, $\sigma_A = 6$ MPa, $h_3 = -1.67\cdot10^{-2}$ MPa.

(C) the viscoplastic potential function

$$\begin{aligned} kF(\sigma,\tau) := {} & \left\{\frac{f_1p_1}{4}\left[-r\frac{\tau}{\sigma_*} - s\left(\frac{\tau}{\sigma_*}\right)^6 + \frac{\sigma}{\sigma_*}\right]^4 \right. \\ & \left\{-\frac{4f_1p_1}{3}\left[-r\frac{\tau}{\sigma_*} - s\left(\frac{\tau}{\sigma_*}\right)^6\right] + \frac{1}{3}(f_2p_1 + f_1p_2)\right\} \\ & \left[-r\frac{\tau}{\sigma_*} - s\left(\frac{\tau}{\sigma_*}\right)^6 + \frac{\sigma}{\sigma_*}\right]^3 + \left\{3f_1p_1\left[-r\frac{\tau}{\sigma_*} - s\left(\frac{\tau}{\sigma_*}\right)^6\right]^2\right. \\ & \left. -\frac{3}{2}(f_2p_1 + f_1p_2)\left[-r\frac{\tau}{\sigma_*} - s\left(\frac{\tau}{\sigma_*}\right)^6\right] + \frac{1}{2}\left(-\frac{\tau}{\sigma_*}p_1 + f_2p_2\right)\right\} \\ & \left[-r\frac{\tau}{\sigma_*} - s\left(\frac{\tau}{\sigma_*}\right)^6 + \frac{\sigma}{\sigma_*}\right]^2 + \left\{-4f_1p_1\left[-r\frac{\tau}{\sigma_*} - s\left(\frac{\tau}{\sigma_*}\right)^6\right]^3\right. \\ & + 3(f_2p_1 + f_1p_2)\left[-r\frac{\tau}{\sigma_*} - s\left(\frac{\tau}{\sigma_*}\right)^6\right]^2 - 2\left(-\frac{\tau}{\sigma_*}p_1 + f_2p_2\right) \\ & \left.\left[-r\frac{\tau}{\sigma_*} - s\left(\frac{\tau}{\sigma_*}\right)^6\right]\right\}\left[-r\frac{\tau}{\sigma_*} - s\left(\frac{\tau}{\sigma_*}\right)^6 + \frac{\sigma}{\sigma_*}\right] \\ & + \left\{f_1p_1\left[-r\frac{\tau}{\sigma_*} - s\left(\frac{\tau}{\sigma_*}\right)^6\right]^4 - (f_2p_1+f_1p_2)\left[-r\frac{\tau}{\sigma_*} - s\left(\frac{\tau}{\sigma_*}\right)^6\right]^3\right. \\ & + \left(-\frac{\tau}{\sigma_*}p_1+f_2p_2\right)\left[-r\frac{\tau}{\sigma_*} - s\left(\frac{\tau}{\sigma_*}\right)^6\right]^2 \\ & \left. + p_2\frac{\tau}{\sigma_*}\left[-r\frac{\tau}{\sigma_*} - s\left(\frac{\tau}{\sigma_*}\right)^6\right]\right\}\ln\left[-r\frac{\tau}{\sigma_*}\right] \\ & \left[-s\left(\frac{\tau}{\sigma_*}\right)^6 + \frac{\sigma}{\sigma_*}\right] - p_2\frac{\tau}{\sigma_*}\frac{\sigma}{\sigma_*}\Big\}\sigma_* + g_0\frac{\tau}{\sigma_*} \\ & + g_1\left(\frac{\tau}{\sigma_*}\right)^2 + g_2\left(\frac{\tau}{\sigma_*}\right)^3 \end{aligned} \tag{13}$$

with
$f_1 = -0.0167$, $p_1 = -1.255\cdot10^{-6}\ s^{-1}$, $g_o = 0.001$ MPa s^{-1}, $f_2 = 0.86$, $p_2 = 6.45\cdot10^{-5}\ s^{-1}$, $g_1 = -8.63\cdot10^{-6}$ MPa s^{-1}, $r = 0.825$, $g_2 = 1.557\cdot10^{-5}$ MPa s^{-1}, $s = 1.37\cdot10^{-8}$, and by definition

$$\frac{\partial F}{\partial \sigma}\Big|_{\sigma \ge \sigma_0} = 0.$$

The shape of several surfaces corresponding to H = constant is shown as a dotted line in Fig. 2 in a $\tau 0\sigma$ plane. In the same figure the surfaces F = constant are shown as dashed lines, the failure surface as a

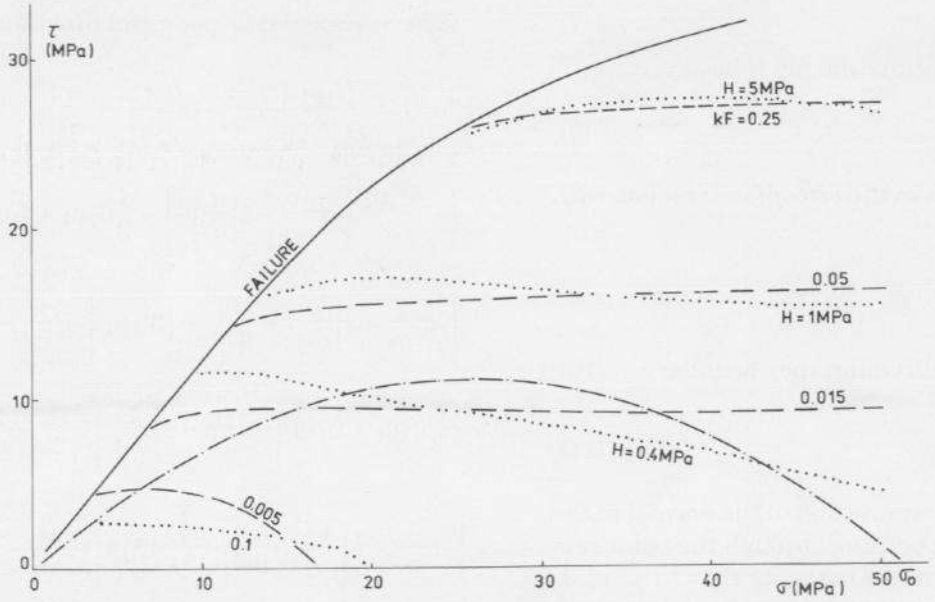

Fig. 2. Surfaces F = const (dashed lines) and H = const (dotted lines), compressibility/dilatancy boundary (dash–dot line) and the failure surface (solid lines) for rock salt.

solid line, while the compressibility/ dilatancy boundary is shown as dash–dot line. Although this boundary passes through the point $\sigma_0 = 51.4$ MPa, from the experimental data it is not certain that the compressibility domain will not extend slightly beyond this point, towards higher pressures (Hunsche, 1991, personal communication), since it is quite difficult to pinpoint the exact value of σ_0.

COMPRESSIBILITY AND DILATANCY AROUND A HORIZONTAL TUNNEL

As a first example, let us examine where, around a tunnel in rock salt, the rock becomes either dilatant or compressible after excavation.

Assuming that the excavation process is a fast one, we will accept that just after excavation the stress distribution is the one obtained from the elastic solution (see, for instance, Cristescu (1989) Ch. 12), i.e. using conventional notation

$$\sigma_{rr} = p\frac{a^2}{r^2} + \frac{1}{2}(\sigma_h + \sigma_v)\left(1 - \frac{a^2}{r^2}\right) + \frac{1}{2}(\sigma_h - \sigma_v)\left(1 - \frac{4a^2}{r^2} + \frac{3a^4}{r^4}\right)\cos 2\theta \qquad (14a)$$

$$\sigma_{\theta\theta} = -p\frac{a^2}{r^2} + \frac{1}{2}(\sigma_h + \sigma_v)\left(1 + \frac{a^2}{r^2}\right) - \frac{1}{2}(\sigma_h - \sigma_v)\left(1 + \frac{3a^4}{r^4}\right)\cos 2\theta \qquad (14b)$$

$$\sigma_{r\theta} = \frac{1}{2}(\sigma_h - \sigma_v)\left(-1 - \frac{2a^2}{r^2} - \frac{3a^4}{r^4}\right)\sin 2\theta \qquad (14c)$$

$$\sigma_{zz} = \sigma_h - \nu(\sigma_h - \sigma_v)\frac{2a^2}{r^2}\cos 2\theta \qquad (14d)$$

where a is the initial radius of the tunnel, (r,θ) are the polar coordinates of any point in the wall, σ_h and σ_v the horizontal and vertical far field (primary) stresses, and p a possible pressure exerted on the wall of the tunnel by a lining or by a fluid existing in the cavity. Concerning the primary stresses, we will assume that σ_v is obtained from the overburden pressure $\sigma_v = \varrho gh = \gamma h$, with the tunnel depth h in meters and stresses in Pa, while for σ_h we choose several variants: $\sigma_h = m\,\sigma_v$ with m = 0.3, 0.5, 0.7 and 1.2.

We introduce (14) into conditions (7)–(11) in order to check which of them is satisfied, the functions H and F being given by (12) and (13). Thus for various depths, it is possible to find the domain around the circumference of the tunnel where the rock becomes dilatant, where compressible, where elastic unloading takes place, and where the failure condition is fulfilled. For instance in Fig. 3a–d, these domains are given for the depth h = 1000 m, for p = 0, and for the four values of m given above. The elastic/viscoplastic boundary is shown as a dotted line, the compressibility/dilatancy boundary is shown as a dash–dot line, the boundary of the domain where failure takes place is marked by a dash/two-dot line, and various lines of constant τ are shown as dotted lines. Here τ is computed from

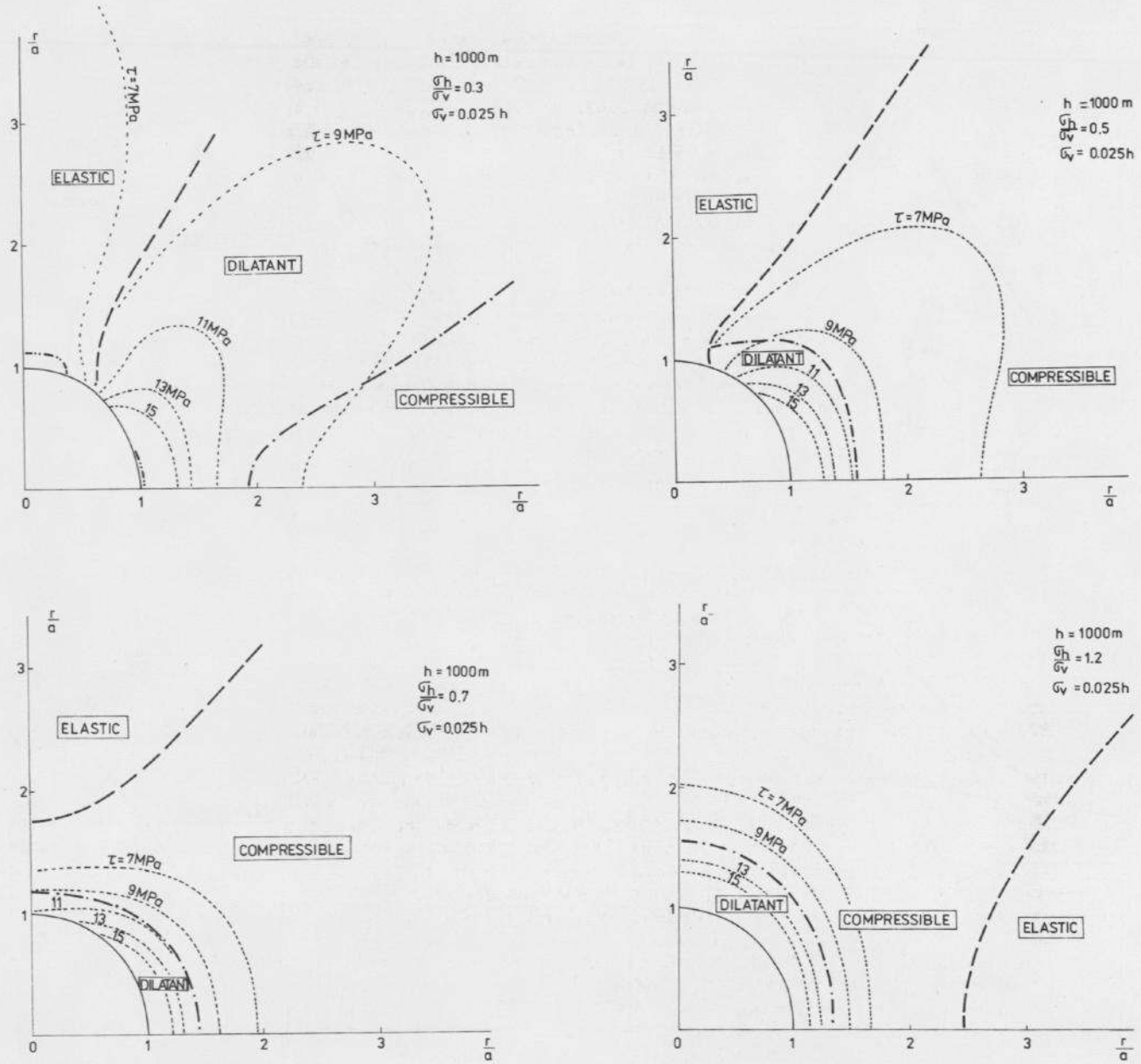

Fig. 3. (a: top left; b: top right; c: bottom left; d: bottom right). Domains of dilatancy, compressibility and elasticity around a tunnel excavated in rock salt at 1 km depth, for four ratios σ_h/σ_v and without internal pressure. Dash/two-dot lines mark domains of failure. The horizontal and vertical axes correspond to horizontal and vertical distances (r) measured radially from the tunnel centre, and normalised with respect to (initial) tunnel radius a.

$$\tau = \frac{\sqrt{2}}{3}\left(\sigma_{rr}^2 + \sigma_{\theta\theta}^2 + \sigma_{zz}^2 - \sigma_{rr}\sigma_{\theta\theta} - \sigma_{\theta\theta}\sigma_{zz} - \sigma_{zz}\sigma_{rr} + 3\,\sigma_{r\theta}^2\right)^{1/2} \qquad (15)$$

using (14). From Fig. 3 it follows that sudden failure is to be expected for relatively small values of the ratio σ_h/σ_v. For higher values of this ratio, failure is not possible. The dilatant domain is adjacent to the excavation, but can extend quite far from it, again if the ratio of the two primary stresses is small. The elastic domain touches the circumference at the crown (mine roof), again for small m, but for m > 1 it approaches only the excavation from the horizontal side.

Figure 4a–d shows similar results obtained for the same values of p and of m, but at the tunnel depth h = 1500 m. This time, failure is present in all cases either at the crown, or at the wall (horizontal direction), or in both directions. In the later case, failure at the crown may be due to tensile stresses. In the present examples both failure domains (i.e at the roof and horizontal direction) have been obtained with a unique failure condition of the form

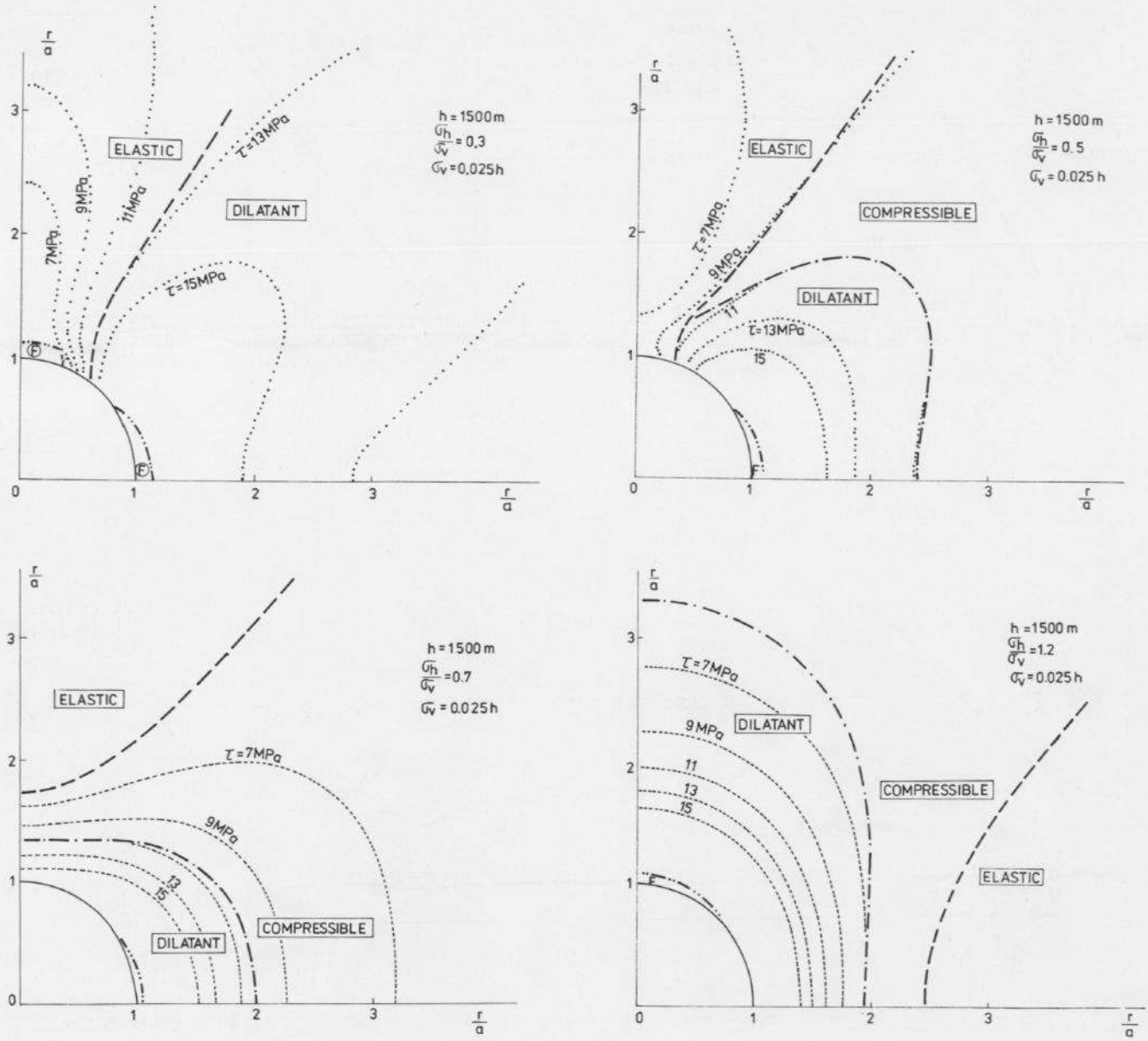

Fig. 4. (a: top left; b: top right; c: bottom left: d: bottom right). As Fig. 3 but at a depth of 1.5 km.

$$-r\frac{\tau}{\sigma_*}-s\left(\frac{\tau}{\sigma_*}\right)^6+\frac{\sigma}{\sigma_*}=0 \qquad (16)$$

incorporated in the expression (13) of the function F, so that when the stress state is approaching a failure state we obtain $\dot{\varepsilon}_v^I \to -\infty$ in the constitutive equation. For tensile stresses ($\sigma < 0$) we could use the alternative failure condition

$$\min \sigma_i = -\sigma_t \qquad (i = 1, 2, 3) \qquad (17)$$

with σ_t the tensile strength of the rock salt and σ_i the principal stress components. In this case, failure will occur at the crown for m = 0.3, but will involve a much smaller domain. Although the two regions of failure shown both mark instantaneous failure, physically they are distinct phenomena. At the crown it is a usual failure in an elastic region (i.e. satisfying a failure condition formulated in terms of stresses, as for instance (16)), while at the wall it is an instantaneous failure due to dilatancy, again satisfying a condition of the same form but bordering on a dilatancy domain; here damage and failure spread slowly into the rock mass with time, as creep-failure by dilatancy (see Cristescu, 1986, 1989).

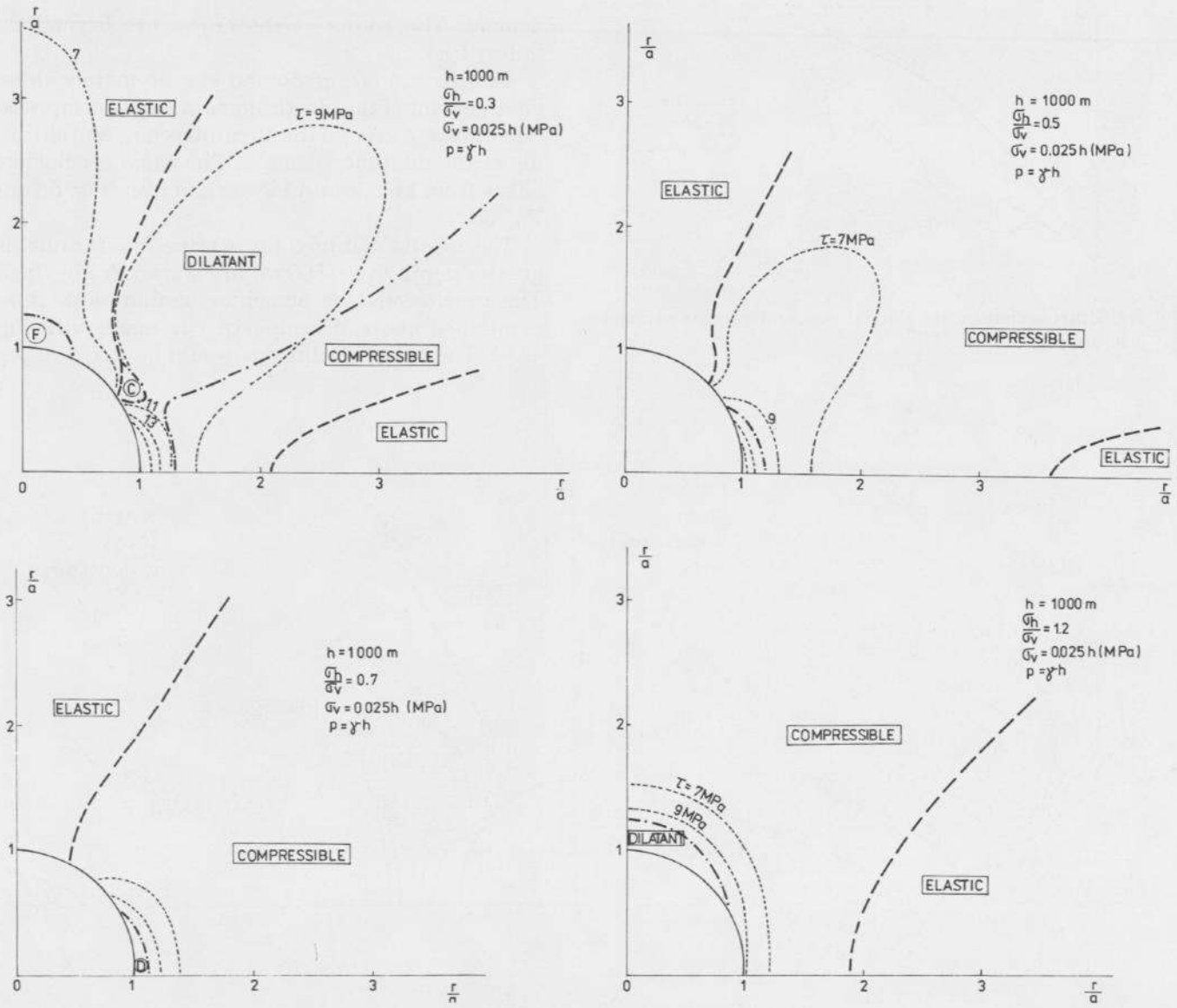

Fig. 5. (a: top left; b: top right; c: bottom left; d: bottom right). As Fig. 3 but with a brine pressure on the walls of the tunnel.

Another conclusion which follows from Fig. 4 as compared with Fig. 3 is that the area covered by the dilatant domain increases with depth.

Figures 3 and 4 have been obtained with the value p = 0 for the internal pressure (empty tunnel). If, however, the tunnel is filled with brine, and the pressure exerted by the brine is the one obtained from the weight of the column of brine (e.g. p = 11772 h (Pa), with h in meters), then all the boundaries of the domain shown above change significantly. For instance, for h = 1000 meters and m = 0.3, Figs. 5a–d show the various existing domains, using the same convention as above for the lines marking the boundaries between domains. If we compare Fig. 5a with Fig. 3a we note that the area of the failure domain at the crown has increased in Fig. 5a, while failure at the wall no longer occurs; the dilatancy domain shrinks and the elastic domain enlarges (both near the circumference and in the horizontal direction). Further, the compressibility domain enlarges and a small additional compressibility domain appears near the contour.

In order to understand better what happens around the circumference, Fig. 6 shows the stress distribution (circles–dashed lines) along the circumference. The primary state is represented by point P; the dotted line represents the surface $H(\sigma) = H(\sigma^P)$ passing through P. Thus, points under this line are in the elastic domain while those above are either in the compressibility or in the dilatancy

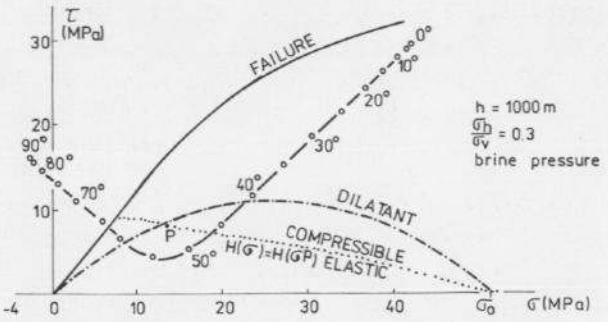

Fig. 6. Stress distribution along the circumference of a tunnel just after excavation.

domain. The points at the crown are beyond the failure line.

Comparison of Fig. 5b and Fig. 3b mainly shows enlargement of the elastic domain and of compressibility domain around the circumference, and shrinking of the dilatancy domain. The same conclusions follow from Fig. 5c and Fig. 3c and from Fig. 5d and Fig. 3d.

The results obtained for a brine-filled tunnel at greater depth (h = 1500 m) are shown in Fig. 7a–d. The conclusions are somehow similar with those mentioned above if comparison is made with Fig. 4a–d. The main conclusions would be that the per-

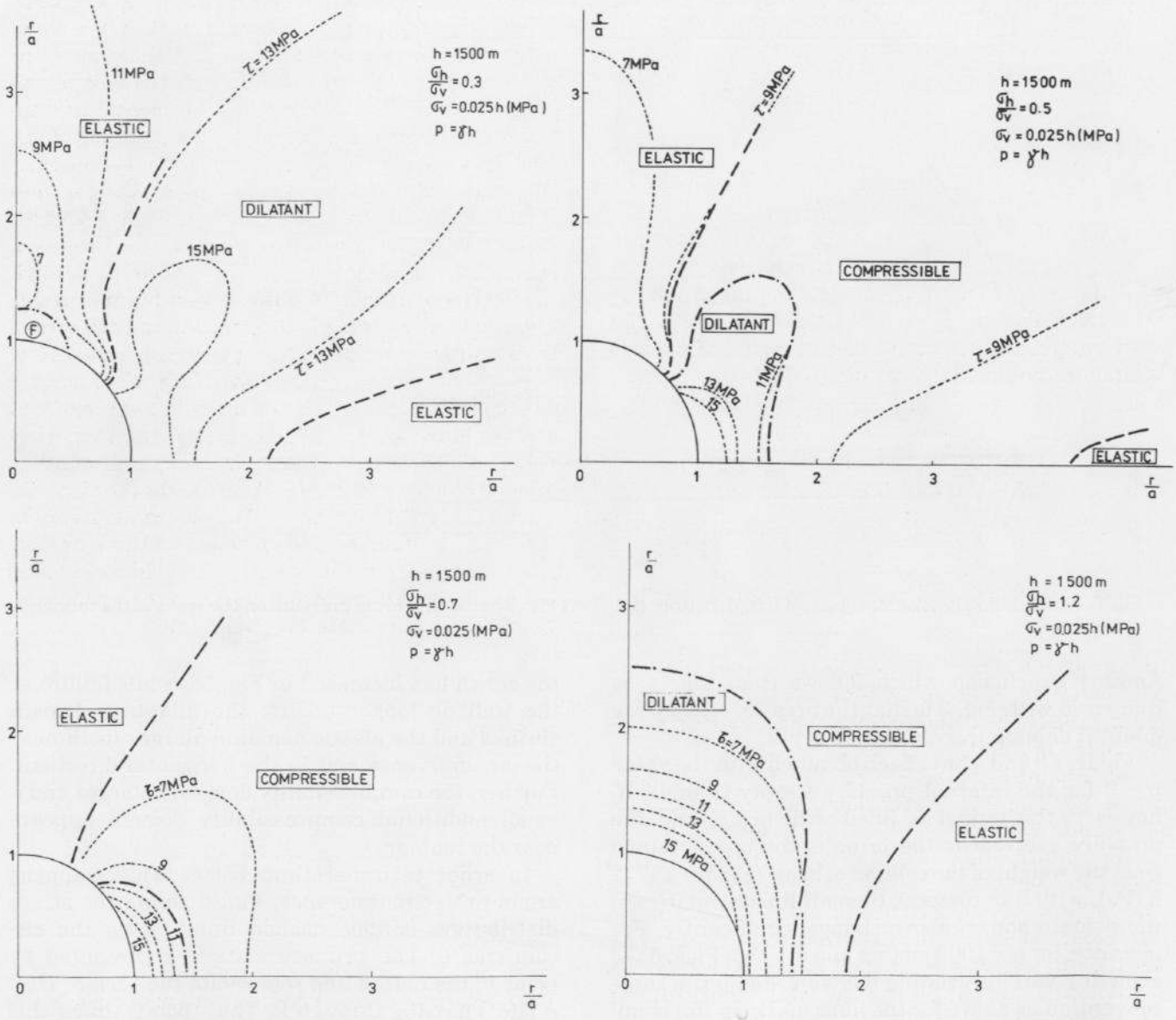

Fig. 7. (a: top left; b: top right; c: bottom left; d: bottom right). As Fig. 3 but at a depth of 1.5 km and with a brine pressure acting on the wall of the tunnel.

formance of the rock salt around the tunnel improves in the presence of the brine pressure, in the sense that failure can be avoided.

CREEP, COMPRESSIBILITY AND/OR DILATANCY AROUND A DEEP VERTICAL CYLINDRICAL CAVERN

The problem of the behaviour of the rock salt around a deep vertical circular cylindrical cavern (or well) can be analysed in a similar way. After the excavation of the cavern, if the excavation takes place in a relatively short time interval as compared to the life span during which the cavern is in use, to a good approximation the stress distribution is the elastic one (see, for instance Cristescu, 1989, Ch. 11)

$$\sigma_r = (p - \sigma_h)\left(\frac{a}{r}\right)^2 + \sigma_h \tag{18a}$$

$$\sigma_\theta = -(p - \sigma_h)\left(\frac{a}{r}\right)^2 + \sigma_h \tag{18b}$$

$$\sigma_z = \sigma_v \tag{18c}$$

After excavation of the cavern, significant creep will occur due to the stress field (18). The radial convergence (u) by creep can be obtained from the simple formula (Cristescu, 1989, Ch.11)

$$\frac{u(r,t)}{a} = -\frac{p-\sigma_h}{2G}\frac{a}{r} + \frac{r}{a}\frac{\left\langle 1 - \frac{W^{IP}}{H}\right\rangle \frac{\partial F}{\partial \sigma_\theta}}{\frac{1}{H}\left(\frac{\partial F}{\partial \sigma}\sigma + \frac{\partial F}{\partial \tau}\tau\right)}\left\{1 - \exp\left[\frac{k}{H}\left(\frac{\partial F}{\partial \sigma}\sigma + \frac{\partial F}{\partial \tau}\tau\right)t_0 - t\right]\right\} \tag{19}$$

if we assume that the stresses (18) stay constant during creep. We remind that Massier (pers. commun., 1984) has demonstrated that for a linear viscoelastic model the stresses are constant during creep around a vertical well. For the viscoplastic model used here the stress constancy during creep is an assumption.

Since the numerical examples which will be given below are for deep caverns, we assume for the far field stresses $\sigma_h = \sigma_v = 0.025$ h, with h in meters and stresses in MPa. W^{IP} involved in (19) is computed for each depth as $W^{IP} = H(\sigma^P, \tau^P)$. The elastic solution is obtained from (19) for $t = t_0$, while the ultimate convergence is obtained for $t \to \infty$, i.e. in the formula (19) the last term (the exponential function) is missing. The speed of convergence is governed by the magnitude of k which is to be determined in creep tests. Since such tests were not available to the author, several values for the dimensionless term $k(t_0 - t)$ will be used in order to give some numerical examples.

Figure 8 shows the convergence of the vertical cavern for the case when no pressure is exerted on the walls (p = 0). The initial, elastic, convergence is quite small and is not shown in the figure. The ultimate convergence u_∞ is quite significant at h >1000 m, while at h > 2000 m complete closure takes place very rapidly (dotted line). At h >1500 m a failure domain around the opening also occurs (solid line). The rock around cavern is compressible at far distances but dilatant near the opening. The compressibility/dilatancy boundary is marked by a dash/dot line. As the depth increases, the dilatancy domain enlarges very significantly and the compressibility/dilatancy boundary has a horizontal asymptote for $\sigma_v = \sigma_0$ (see also Fig. 2 for the meaning of σ_0).

If the vertical cavern is filled with brine, the radial convergence of the walls is much smaller and complete closure by creep is obtained at a greater depth (Fig. 9). The pressure exerted by the brine was computed according to p = 11772 h, with the depth h in meters and p in Pa. No failure was obtained in this case, and the domain of dilatancy around the cavern is significantly reduced. The progressive closure of the bottom of the cavern is shown for various successive moments in time. Since a precise value of k is still pending good creep data, several numerical values were attributed to the dimensionless quantity $k(t - t_0)$ as shown in Fig. 9. If we use for the viscosity coefficient the value $E/k = 10^{17}$ Poise as given by Albrecht and Langer (1974), then the three convergence curves shown in the Fig. 9 would correspond to 38.6 days, 193 days and 10.5 years respectively. These figures are certainly preliminary.

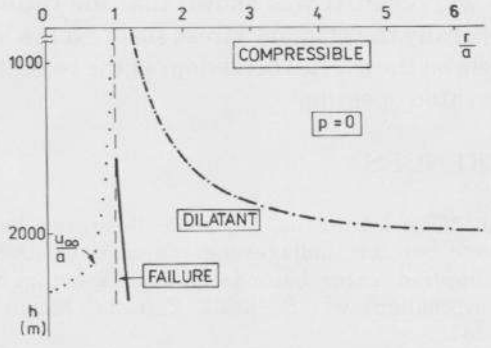

Fig. 8. Domains of dilatancy and compressibility around a deep empty vertical cavern; the solid line marks failure and the dotted line ultimate convergence of the walls.

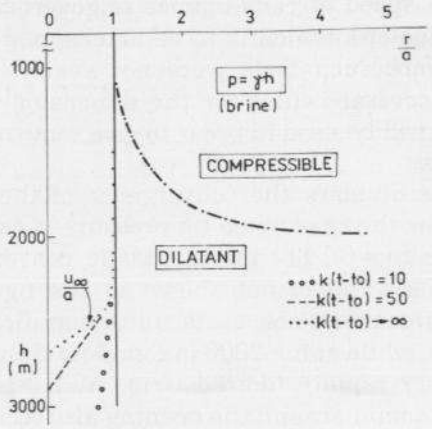

Fig. 9. Domains of dilatancy and compressibility around a deep vertical cavern filled with brine; circle/line, interrupted line, and dotted line mark successive positions during convergence of the walls.

CONCLUSIONS

Starting from a complete set of true triaxial test data, one can formulate directly a general phenomenological constitutive equation, able to describe creep, dilatancy and/or compressibility, work-hardening, damage and creep-failure. No preliminary uniaxial model is necessary for the formulation of the general constitutive equation. Since the data used here were obtained in short-term tests, subsequent creep tests are necessary mainly to make precise the magnitude of the viscosity coefficient. Also, it is necessary to include long-term stationary creep in a future variant of the model, in order to improve the description of the creep phenomenon.

With a general formulation of the constitutive equation it is very easy to predict where, around a horizontal tunnel or vertical cavern, the rock will become dilatant, where compressible, or where failure will occur. It was shown that the ratio σ_h/σ_v and generally the primary stress state exert a significant role on the overall behaviour of the rock around an excavated opening.

REFERENCES

Albrecht, H. and Hunsche, U., 1980. Gebirgsmechanische Aspekte bei der Endlagerung radioaktiver Abfälle in Salzdiapiren unter besonderer Berücksichtigung des Fliessverhaltens von Steinsalz. Fortschr. Miner. 58(2): 212–247.

Albrecht, H. and Langer, M., 1974. The rheological behaviour of rock salt and related stability problems of storage caverns. Proc. 3rd Congr. Int. Soc. Rock Mech., Denver, Vol. 2, Part B: 967–974.

Aubertin, M., Gill, D.E. and Ladanyi, B., 1989. The active stress concept and the creep of rock salt. Proc. Sixth Int. Congr. on Rock Mechanics, Montreal 1987, Balkema, 3: 1501–1503.

Aubertin, M., Gill, D.E. and Ladanyi, B., 1991. A unified visco-plastic model for the inelastic flow of alkali halides, Mech. Materials 11: 63–82.

Blum, W., Vogler, S., Biberger, M. and Mukherjee, A.K., 1989. Stress Dependence of the Creep Rate at Constant Dislocation Structure. Mat. Sc. Eng. A112: 93–106.

Cristescu, N., 1986. Damage and failure of viscoplastic rock-like materials. Int. J. Plasticity, 2: 189–204.

Cristescu, N., 1987. Elastic-viscoplastic constitutive equations for rock. Int. J. Rock Mech. Sci. and Geomech. Abstr., 24: 271–282.

Cristescu, N., 1989. Rock Rheology. Kluwer Academic Publ., Dordrecht, Boston, London, 336 pp.

Cristescu, N., 1991. Nonassociated elastic/viscoplastic constitutive equations for sand. Int. J. Plasticity, 7: 41–64.

Cristescu, N., 1992. Rock Rheology. In: Comprehensive Rock Engineering, Ch. 21, Pergamon Press.

Cristescu, N., 1993. A procedure to determine nonassociated constitutive equations for geomaterials. Int. J. Plasticity, 9 (submitted).

Cristescu, N. and Hunsche, U., 1991. A constitutive equation for salt. Proc. 7th Int. Congr. on Rock Mechanics, Aachen, Sept.1991.

Cristescu, N. and Hunsche, U., 1992. Determination of a Nonassociated Equation for Rock Salt from Experiments. Proc. IUTAM-Symposium 1991, Hannover. Springer, Berlin. pp. 511–523.

Desai, C.S. and Varadarajan, A., 1987. A constitutive model for quasistatic behavior of rock salt. J. Geophys. Res., 92, B11: 11445–11456.

Dreyer, W., 1973. The Science of Rock Mechanics; Part 1. Trans. Tech Publ. Clausthal-Zellerfeld, 500 pp.

Horsemann, S. and Passaris, E., 1984. Creep test for storage cavity closure prediction. In: H.R. Hardy and M. Langer (Editors) First Conf. Mech. Behavior of Salt. Trans Tech Publ., Clausthal-Zellerfeld. pp. 120–157.

Hunsche, U., 1990a. On the fracture behavior of rock salt. In: A.S. Krausz, J.I. Dickenson, J.-P.A. Immarigson, and W. Wallace (Editors). Constitutive Laws of Plastic Deformation and Fracture. Proc. 19th Canadian Fracture Conf. Ottawa, Kluwer Acad. Publ., Dordrecht, pp. 155–163.

Hunsche, U., 1990b. A failure criterion for natural polycrystalline rock salt. In: Fan Jinghong and S. Murakami (Editors). Advances in Constitutive Laws for Engineering Materials. Proc. ICCLEM. International Academic Publ., Vol. 2. pp. 1043–1046.

Hunsche, U., 1991. Volume change and energy dissipation in rock salt during triaxial failure tests. In: Proc. of Mechanics of Creep Brittle Materials. Leichester Sept. 1991. Elsevier, Amsterdam.

Hunsche, U. and Cristescu, N., 1993. Constitutive equation for rock salt — A new approach.

Langer, M., 1984. The Rheological Behavior of Rock Salt. In: H.R. Hardy and M.Langer (Editors). First Conf. Mech. Behavior of Salt. Trans Tech Publ., Clausthal. pp. 201–240.

Munson, D.E. and Dawson, P.R., 1984. Salt constitutive modeling using mechanics maps. In: H.R. Hardy and M. Langer (Editors). First Conf. Mech. Behavior of Salt. Trans Tech Publ., Clausthal. pp. 717–737.

Serata, S., Sakurai, S. and Adachi, T., 1972. Theory of aggre-

gate rock behavior based on absolute three-dimensional testing (ATT) of rock salt. In: K.E. Gray (Editor). Basic and Applied Rock Mechanics. The Amer. Inst. Mining, Metallurgical and Petroleum Engineers Inc., New York. pp. 431–473.

Spiers, C.J. and Schutjens, P.M.T.M., 1990. Densification of crystalline aggregates by fluid-phase diffusional creep. In: D.J. Barber, P.G. Meredith (Editors), Deformation Processes in Minerals, Ceramics and Rocks, UNWIN HYMAN, Boston, Sydney, Wellington. pp. 334–353.

Vogler, S. and Blum, W., 1990. Micromechanical Modelling of Creep interms of the Composite Model. Fourth Int. Conf. on Creep and Fracture of Engineering Materials and Structures. Swansea, April 1990 (Preprint).

Wawersik, W.R., Herrmann, W., Montgomery, S.T. and Lauson, R.S., 1982. Excavation design in rock salt — Laboratory experiments. In: W. Wittke (Editor). Material modeling and validations. ISRM Symposium. Balkema, Rotterdam. pp. 1345–1356.

Wawersik, W.R. and Zeuch, D.H., 1986. Modeling and mechanistic interpretation of creep of rock salt below 200°C. Tectonophysics, 121: 125–152.